First-Order Interfacial Transformations with a Critical Point: Breaking the Symmetry at a Symmetric Tilt Grain Boundary

Shengfeng Yang, Naixie Zhou, Hui Zheng, Shyue Ping Ong, and Jian Luo

Phys. Rev. Lett. **120**, 085702 — Published 22 February 2018

DOI: 10.1103/PhysRevLett.120.085702

First-Order Interfacial Transformations with a Critical Point: Breaking the Symmetry at a Symmetric Tilt Grain Boundary

Shengfeng Yang, Naixie Zhou, Hui Zheng, Shyue Ping Ong, Jian Luo[*]

Department of NanoEngineering, University of California, San Diego, La Jolla, CA 92093, USA

Abstract:

First-order interfacial phase-like transformations that break the mirror symmetry of the symmetric ∑5 (210) tilt grain boundary (GB) are discovered by combining a modified genetic algorithm with hybrid Monte Carlo and molecular dynamics simulations. Density functional theory calculations confirm this prediction. This first-order coupled structural and adsorption transformation, which produces two variants of asymmetric bilayers, vanishes at an interfacial critical point. A GB complexion (phase) diagram is constructed via semi-grand canonical ensemble atomistic simulations for the first time.

[*] Corresponding author. E-mail address: jluo@alum.mit.edu (J. Luo).

Solute adsorption (*a.k.a.* segregation) at grain boundaries (GBs) can induce interfacial phase-like structural transformations [1-3] that can abruptly change a spectrum of physical properties of polycrystalline materials [1-12]. Despite their great importance [1,2,9,13], it remains a major scientific challenge to predict, as well as discover new types of, interfacial phase-like behaviors. Unfortunately, atomic-resolution experimental characterizations of GBs as a function of both bulk composition and temperature to systematically map out the stability and transformation of 2-D interfacial phases (that are also called "complexions" [1,3,14,15]) are often infeasible. By combining a modified genetic algorithm (GA) with hybrid Monte Carlo (MC) and molecular dynamics (MD) simulations, we discover a new type of interfacial phase transformation that breaks the mirror symmetry of a symmetric tilt GB, as well as an interfacial critical point and the effects of premelting/prewetting like interfacial disordering at high temperatures. The breaking of the mirror symmetry also implies the existence of two variants of the high-adsorption complexion, represented by the asymmetric bilayer adsorption of Ni. We further demonstrate the feasibility of constructing a temperature- and composition-dependent GB 'phase' (complexion) diagram through semi-grand canonical ensemble atomistic simulations, with potentially broad implications.

On one hand, a series of recent studies [6,16-18] extended bulk CALPHAD (calculation of phase diagrams) methods to model coupled GB premelting and prewetting and subsequently constructed GB λ diagrams to represent the thermodynamic tendency for average general GBs to disorder. Such GB diagrams have been validated experimentally [6,16,17,19-21] and used to forecast sintering behaviors [6,16,18,19,22-24]. Moreover, diffuse-interface (phase-field) [11,14,15] and lattice-type [25-28] models have been used to compute more rigorous GB complexion (phase) diagrams with first-order transition lines and critical points. Yet, these phenomenological thermodynamic models cannot represent all atomic details realistically.

On the other hand, atomistic simulations can provide great structural details underlying the GB transformations. Notably, a segregation-induced GB transformation from a "split-kite" phase to a "filled-kite" phase at the $\sum 5$ (210) tilt GB in Ag-doped Cu has been observed with MC simulations [10]. Interfacial transformations from ordered GBs to disordered nanoscale intergranular films in Zr-doped Cu GBs have also been studied using atomistic simulations [29-31]. While these prior studies provided important atomic details for the GB structures and their

transformations, GB complexion (phase) diagrams with well-defined first-order transition lines and critical points have not yet been constructed by atomistic simulations.

In this study, the ∑5 (210) / [001] symmetric tilt GB in Ni-doped Mo is modeled via a new methodology that combines a modified GA with subsequent hybrid MC/MD simulations to predict the equilibrium GB structure as a function of temperature and bulk composition. We discover a first-order GB phase-like transformation that breaks the mirror symmetry of the symmetric tilt GB. This first-order coupled structural and adsorption transition interplays with interfacial disordering with increasing temperature, and it vanishes at an interfacial critical point. Subsequently, we construct the first GB complexion (phase) diagrams through semi-grand canonical ensemble atomistic simulations.

First, we implement and further modify a GA [32-34], which is an adaptive heuristic search algorithm based on the evolutionary ideas of natural selection and genetics, to search for the lowest-energy GB structure through the energy landscape at 0K. The details of this modified GA are described in the Supplemental Materials. Compared with the traditional GA [32-34], we add an extra step of "species change" in this modified GA (Supplemental Fig. S1). During this step, the species of atoms are exchanged following a similar procedure in MC simulation to consider solute adsorption at GBs in semi-grand canonical ensembles. In the step of tournament selection, energy evaluation is modified by introducing the chemical potential difference between Ni and Mo into the total free energy of GB at 0 K. In this work, we have fifty GBs in each generation, and the GA searches typically converge within one hundred generations.

Second, hybrid MC/MD simulations [35,36], using the GB atomic structures obtained from GA at 0 K as initial structures, are subsequently performed to investigate the equilibrium structures of Ni-doped Mo GBs at finite temperatures. The atomic structural relaxations are realized by MD running, and the MC scheme samples the semi-grand canonical ensemble. LAMMPS [37] is used to perform the hybrid MC/MD at zero hydrostatic pressure using Berendsen's thermostat and barostat. During the simulation, five MC trial moves are performed between each MD step; equivalently, 4,075 MD steps are performed per MC cycle [equivalent to N_{at} MC trial moves, where N_{at} (= 20,376) is the number of atoms in our simulations]. MC swaps of Ni atoms with Mo atoms are performed, and the swap probability is dictated by the Metropolis criterion in specified temperatures. All atoms move according to the regular MD time integration

and the time step is 0.0001 picoseconds. The hybrid MC/MD simulation is considered to reach an equilibrium if the fluctuation of total energy over the last 10,000 steps is less than 0.5%. The simulations typically take approximately 1 million MD steps for the system to converge. Hybrid MC/MD simulations can produce more accurate and efficient predictions of equilibrium GB structures because the initial structure obtained by the GA search over a large energy landscape is more accurate (see, *e.g.*, Supplemental Fig. S2 for a comparison with the experiment [38] for the undoped GB).

The ∑5 (210) / [001] symmetric tilt GB in Ni-doped Mo was modeled in this study, where the periodic boundary conditions were used in all three directions. The computational model is 200.00 Å long, 84.44 Å tall, and 18.88 Å thick, and there were 20,376 atoms (Supplemental Fig. S2). An embedded atom method (EAM) potential for Mo-Ni alloy [39] was used in this work. This potential performs better than the only other available interatomic potential in terms of predicting the effect of Ni dopant on the energy of Mo GB (as shown in Supplemental Fig. S7). The Mo-Ni bulk phase equilibrium conditions (for this MD potential) were calculated by using a similar calculation procedure to the one used in the Ag-doped Cu system [40]. All the simulated temperatures in this work were normalized by dividing the temperature by the simulated melting temperature (T_m = 3750K) of pure Mo.

Figure 1 shows a GB phase-like transformation identified in the hybrid MC/MD simulations with increasing chemical potential difference $\Delta\mu_{Ni}$ ($\equiv \mu_{Ni} - \mu_{Ni}^{(pure)}$) at a constant temperature of $T = 0.373\ T_m$. The initial state of $\Delta\mu_{Ni} = -0.56$ eV/atom (1 eV/atom = 96.521 kJ/mol) of this GB is a nominally "clean" GB (Fig. 1(a)). A bilayer complexion (with nominally two adsorbed atomic layers of Ni) starts to form with increasing $\Delta\mu_{Ni}$. Figure 1(b) shows the coexistence of "clean" and bilayer complexions at the transforming $\Delta\mu_{Ni}$ of -0.435 eV/atom. When $\Delta\mu_{Ni}$ reaches -0.385 eV/atom, the GB has been fully transformed to a bilayer complexion (Fig. 1(c)).

The atomistic simulations were performed for a large number of alloys with different compositions at different temperatures to construct GB diagrams to represent both interfacial excess adsorption and disorder. Fig. 2(a) shows a computed map of the GB Gibbs excess (net adsorption) of Ni, in which the color of each data point represents the averaged GB adsorption amount (Γ_{Ni}) at that specific temperature and bulk composition. We used the equivalent number of (210) monolayers to represent the Ni adsorption (Γ_{Ni}); the segregation amount of one (210)

monolayer is equivalent to ~4.5 atom/nm^2. The GB adsorption at each bulk composition and temperature was obtained by averaging the computed Γ_{Ni}'s from ten equilibrated atomic configurations at the same bulk composition and temperature to ensure statistical accuracies. These ten configurations are selected at every 10,000 timesteps after the convergence criterion has been met.

After an atomic GB structure had been obtained from hybrid MC/MD simulations, the disorder parameter for each atom in the specimen was computed by using a bond-orientational [34] disorder parameter *d*. This parameter measures the similarity of the local atomic surrounding of a given atom with that of its neighboring atoms. The disorder parameter equals to zero for atoms situated in a perfect lattice and equals to one for atoms in the liquid phase. The calculation procedure of disorder parameter is similar to the one used by Chua *et al.* [34] and Steinhardt *et al.* [41]. The GB excess in disorder parameter for each GB configuration was calculated using $\Gamma_d \equiv (\sum_{i=1}^{N} d_i^{GB} - \sum_{i=1}^{N} d_i^{Grain})/A$, where A is the GB area, N is the number of atoms in the computation cell (with or without a GB), and $\sum_{i=1}^{N} d_i^{GB}$ and $\sum_{i=1}^{N} d_i^{Grain}$ are the sums of disorder parameters of all atoms in the computation cell containing the GB and a reference cell in the grain interior without a GB, respectively (Supplemental Fig. S3). After calculating the GB excesses in disorder for the equilibrated interfacial structures at various grain compositions and temperatures, a computed map of GB excess in disorder is constructed and plotted in Fig. 2(b). In general, the GB adsorption of Ni (Γ_{Ni}) increases and the GB structure becomes more disordered with the increasing bulk composition or temperature (Fig. 2).

From the computed GB diagrams, we have identified a first-order phase-like transformation line (the solid purple line in Fig. 2) from normally "clean" GBs to the bilayer complexion. This first-order phase-like transformation is further illustrated in Fig. 3(a), as evident by the abrupt "jumps" in GB excess in Ni (Γ_{Ni}) *vs.* chemical potential difference ($\Delta\mu_{Ni} \equiv \mu_{Ni} - \mu_{Ni}^{(pure)}$) curves at $T = 0.4\ T_m$ obtained by hybrid MC/MD and at $T = 0$K obtained by the modified GA, respectively. Four corresponding snapshots are shown in Fig. 3(b).

Specifically, the first-order transformation reproduced by the modified GA at 0 K shown in the black dashed line in Fig. 3(a) corresponds exactly to a discontinuous "jump" from "$\Gamma_{Ni} = 0$" to "$\Gamma_{Ni} = 2$ monolayers" at $\Delta\mu_{Ni} \approx -0.35$ eV/atom. This first-order transformation was found to

be a coupled chemical (adsorption) and structural transition that breaks the mirror symmetry of the otherwise symmetric tilt GB from the analysis of the atomic GB structures. The bottom row of Panel ③ and Panel ④ in Fig. 3(b) show the 0K atomic structures obtained by the modified GA search; they illustrate that the adsorption transition from "$\Gamma_{Ni} = 0$" to "$\Gamma_{Ni} = 2$ monolayers" accompanies a structural transition that breaks the symmetry in two aspects: (1) the adsorption induces a translation of the two abutting grains by a distance of $0.3a_{bcc}$ (where a_{bcc} is the BCC lattice parameter) along the vertical direction (plus $0.21a_{bcc}$ in the horizonal direction so that the two grains are closer; no translation perpendicular to the projection plane) in Fig. 3(b) and (2) while one adsorption layer of Ni is on the original mirror plane of the symmetric tilt GB, the other Ni layer is asymmetrically adsorbed on (only) one side of one abutting grain. At finite temperatures, the asymmetric bilayers become more disordered (Panel ② in Fig. 3(b)).

With the occurrence of this first-order transition, the GB structure can transition to one of the two equivalent GB configurations or variants of the asymmetric bilayer adsorption of Ni (with the same amount of adsorption and a mirror symmetry to each other, albeit disorders at finite temperatures). Thus, 2-D "anti-phase GB domains" of these two variants with "anti-phase boundary lines" may in principle exist at the same GB after the occurrence of this coupled adsorption and structural transition.

In order to verify the existence of this observed first-order phase-like transformation that breaks the symmetry, we carried out DFT calculations using projector augmented wave (PAW) [42] method as implemented in the Vienna *Ab Intio* Simulation Package [43]. A plane-wave energy cutoff of 400 eV and the Perdew-Burke-Ernzerhof (PBE) generalized gradient approximation (GGA) functional [44] were used. For Brillouin zone (BZ) integration, a Gamma centered grid with a (10×4×1) was used according to the lattice parameters: $a = 3.15$, $b = 7.04$, $c = 54.00$ with the unit Å. The convergence criteria were 5×10^{-4} eV for energy and 0.02 eV/Å for the force. All the calculations were spin-polarized. We created the atomic models with 78 atoms as the initial structures for DFT calculations. In total, we created five different GB models. The first one was the "clean" model to represent the ∑5 (210) / [001] Mo GB without any solutes. The asymmetric bilayer model shown in Fig. 4(b) is obtained from the modified GA. To investigate other possible structural changes (*i.e.*, the stability of the observed translation between two grains), we created three additional models (*i.e.*, M1, M2, M3 in Fig. 4(c)-(e)) by

placing the solutes at different sites near the GB in the "clean" GB model. After relaxation by DFT calculations, we computed and compared the energy difference of all the five different GB models. As shown in Fig. 4(a), we found the bilayer model has the lowest energy compared to the other three models (M1, M2, and M3), verifying the necessity of the structural change and translation to achieve a stable bilayer GB. Moreover, Fig. 4(a) also shows that the "clean" GB transits to the bilayer GB with the increasing chemical potential difference $\Delta\mu_{Ni}$ (but the transformation occurs at a lower $\Delta\mu_{Ni}$, which is presumably a result of the difference in the interatomic interactions in DFT calculations and the EAM potential). In summary, the DFT calculations agree with the modified GA and hybrid MC/MD simulations qualitatively, and verify the occurrence of the first-order coupled structural and adsorption transformation that breaks the symmetry at 0K.

Similar first-order phase-like transformations were observed in hybrid MC/MD simulations at finite temperatures. Fig. 3(a) shows that the threshold $\Delta\mu_{Ni}$ for the first-order transformation in the hybrid MC/MD simulation at $0.4T_m$ is smaller than that obtained by the modified GA at 0 K, where both the "clean" GBs and asymmetric bilayers become nominal (with Γ_{Ni} values being close to, but exactly at, 0 and 2 monolayers, respectively). Moreover, the interfacial structures shown in top row of Panel ① and Panel ② at 0.4 T_m are also more disordered than those in the bottom row of Panel ③ and Panel ④ at 0K in Fig. 3(b), which correspond to increasing interfacial disorder (Γ_d) at high temperatures (Fig. 2(b)). Fig. 3(c) further plots the Γ_{Ni} *vs.* $\Delta\mu_{Ni}$ curves computed by hybrid MC/MD at four different temperatures, showing that the transition becomes smoother with the increasing temperature. The first-order transition becomes continuous above an interfacial critical point at ~$0.56T_m$.

We also compared GB diagrams obtained from atomistic simulations with those computed using two simplified thermodynamic models. Using a Wynblatt-Chatain type lattice model [25], we computed a GB adsorption diagram for a symmetric twist GB without considering the effects of interfacial disordering (Supplemental Fig. S4(a)). A similar first-order transition line and a critical point are also evident in the lattice model. We further compared the Γ_{Ni} *vs.* $\Delta\mu_{Ni}$ curves at four different temperatures (Supplemental Fig. S5). While both atomistic simulations and lattice model show similar trends, higher levels of adsorptions are observed in the atomistic simulations at high temperatures and/or high (less negative) $\Delta\mu_{Ni}$, which are presumably because of

interfacial disordering at high temperatures/segregation levels that can promote more adsorption (in a positive feedback loop), but are not considered in the lattice model. To evaluate the interfacial disordering at high temperatures, we computed a GB λ diagram (Supplemental Fig. S4(b)) using the thermodynamic model in Ref. [6] to forecast coupled GB prewetting and premelting without atomistic details. A comparison between the GB λ diagram (Supplemental Fig. S4(b)) and Fig. 2(a) and (b) from atomistic simulations show that the GB λ diagram can represent the general trends of both adsorption and interfacial disordering, particularly at high temperatures and/or $\Delta\mu_{Ni}$ (close to the solidus line) but without atomistic details (nor any first-order transformations). In summary, Fig. 2(a) and (b) from atomistic simulations can represent both the first-order adsorption transition from the lattice model at low temperature and coupled prewetting and premelting behaviors at high temperature (or close to the solidus line). The atomistic simulations are more realistic and accurate and can discover new phenomena, *e.g.*, the symmetry breaking, that cannot be captured by simplified thermodynamic models.

In conclusion, we have identified a first-order GB phase-like transformation that breaks the mirror symmetry of the symmetric tilt GB at 0K in Ni-doped Mo, along with associated effects of premelting/prewetting like high-temperature interfacial disordering and an interfacial critical point. This first-order adsorption transition is coupled with an asymmetric GB structural transition, producing two variants of asymmetric bilayer adsorption of Ni. Moreover, we have demonstrated the feasibility of constructing a GB diagram by semi-grand canonical ensemble atomistic simulations. The simulation results have been verified by DFT calculations and critically compared with two simplified phenomenological thermodynamic models. Because 2-D interfacial phase behaviors and critical phenomena can affect a spectrum of physical properties of various materials, the new discoveries made by a combination of a modified GA, hybrid MC/MD simulations, and DFT calculations, as well the newly-demonstrated feasibility of constructing GB phase (complexion) diagrams via atomistic simulations, can have broad scientific and technological impacts.

The authors gratefully acknowledge the support from a Vannevar Bush Faculty Fellowship sponsored by the Basic Research Office of the Assistant Secretary of Defense for Research and Engineering and funded by the Office of Naval Research through grant N00014-16-1-2569.

Reference:

[1] P. R. Cantwell, M. Tang, S. J. Dillon, J. Luo, G. S. Rohrer, and M. P. Harmer, Acta Materialia **62**, 1 (2014).
[2] T. Frolov and Y. Mishin, Journal of Chemical Physics **143**, 044706 (2015).
[3] W. D. Kaplan, D. Chatain, P. Wynblatt, and W. C. Carter, Journal of Materials Science **48**, 5681 (2013).
[4] S. J. Dillon, M. Tang, W. C. Carter, and M. P. Harmer, Acta Materialia **55**, 6208 (2007).
[5] J. Luo, Corrosion **72**, 897 (2015).
[6] J. Luo, Journal of the American Ceramic Society **95**, 2358 (2012).
[7] J. Luo, Critical Reviews in Solid State and Material Sciences **32**, 67 (2007).
[8] J. Luo, Journal of Materiomics **1**, 22 (2015).
[9] T. Frolov, M. Asta, and Y. Mishin, Current Opinion in Solid State and Materials Science **20**, 308 (2016).
[10] T. Frolov, M. Asta, and Y. Mishin, Physical Review B **92**, 5, 020103 (2015).
[11] Y. Mishin, W. J. Boettinger, J. A. Warren, and G. B. McFadden, Acta Materialia **57**, 3771 (2009).
[12] T. Frolov, S. V. Divinski, M. Asta, and Y. Mishin, Phys. Rev. Lett. **110**, 255502 (2013).
[13] P. Lejček, M. Šob, and V. Paidar, Progress in Materials Science **87**, 83 (2017).
[14] M. Tang, W. C. Carter, and R. M. Cannon, Physical Review B **73**, 024102 (2006).
[15] M. Tang, W. C. Carter, and R. M. Cannon, Physical Review Letters **97** (2006).
[16] X. M. Shi and J. Luo, Physical Review B **84**, 14, 014105 (2011).
[17] X. M. Shi and J. Luo, Applied Physics Letters **94**, 3, 251908 (2009).
[18] X. M. Shi and J. Luo, Physical Review Letters **105**, 4, 236102 (2010).
[19] N. Zhou and J. Luo, Acta Materialia **91**, 202 (2015).
[20] V. K. Gupta, D. H. Yoon, H. M. Meyer, and J. Luo, Acta Materialia **55**, 3131 (2007).
[21] J. Luo, V. K. Gupta, D. H. Yoon, and H. M. Meyer, Applied Physics Letters **87**, 231902 (2005).
[22] J. Luo and X. M. Shi, Applied Physics Letters **92**, 3, 101901 (2008).
[23] J. Luo, Current Opinion in Solid State and Materials Science **12**, 81 (2008).
[24] N. X. Zhou, T. Hu, and J. Luo, Curr Opin Solid St M **20**, 268 (2016).
[25] P. Wynblatt and D. Chatain, Materials Science and Engineering A **495**, 119 (2008).
[26] J. Luo, Applied Physics Letters **95**, 071911 (2009).
[27] J. M. Rickman, H. M. Chan, M. P. Harmer, and J. Luo, Surf Sci **618**, 88 (2013).
[28] J. M. Rickman and J. Luo, Curr Opin Solid St M **20**, 225 (2016).
[29] Z. L. Pan and T. J. Rupert, Physical Review B **93**, 15, 134113 (2016).
[30] Z. Pan and T. J. Rupert, Computational Materials Science **131**, 62 (2017).
[31] Z. Pan and T. J. Rupert, Scripta Materialia **130**, 91 (2017).
[32] J. Zhang, C. Z. Wang, and K. M. Ho, Physical Review B **80** (2009).
[33] A. Kaczmarowski, S. J. Yang, I. Szlufarska, and D. Morgan, Computational Materials Science **98**, 234 (2015).
[34] A. L. S. Chua, N. A. Benedek, L. Chen, M. W. Finnis, and A. P. Sutton, Nature Materials **9**, 418 (2010).
[35] B. Sadigh, P. Erhart, A. Stukowski, A. Caro, E. Martinez, and L. Zepeda-Ruiz, Physical Review B **85**, 184203 (2012).
[36] S. Jonathan, S. Alexander, and A. Karsten, Acta Materialia **59**, 29572968 (2011).
[37] S. Plimpton, Journal of Computational Physics **117**, 1 (1995).
[38] M. Bacia, J. Morillo, J. M. Penisson, and V. Pontikis, Philos. Mag. A-Phys. Condens. Matter Struct. Defect Mech. Prop. **76**, 945 (1997).
[39] X. W. Zhou, R. A. Johnson, and H. N. G. Wadley, Physical Review B **69** (2004).

[40] P. L. Williams, Y. Mishin, and J. C. Hamilton, Modelling and Simulation in Materials Science and Engineering **14**, 817 (2006).
[41] J. S. Paul, R. N. David, and R. Marco, Physical Review B **28**, 784805 (1983).
[42] P. E. Blochl, Phys. Rev. B **50**, 17953 (1994).
[43] G. Kresse and J. Furthmuller, Phys. Rev. B **54**, 11169 (1996).
[44] J. P. Perdew, K. Burke, and M. Ernzerhof, Phys. Rev. Lett. **77**, 3865 (1996).
[45] See Supplemental Material [please insert url] for Supplemental Figs. S1-S7, a description of the modified Genetic Algorithm, and calculated segregation energies, which includes Refs. [32-34, 37, 41, 46-47].
[46] R. Tran, Z. H. Xu, N. X. Zhou, B. Radhakrishnan, J. Luo, and S. P. Ong, Acta Mater. **117**, 91 (2016).
[47] Q. Zhang, W. S. Lai, and B. X. Liu, Phys. Rev. B **58**, 14020 (1998).

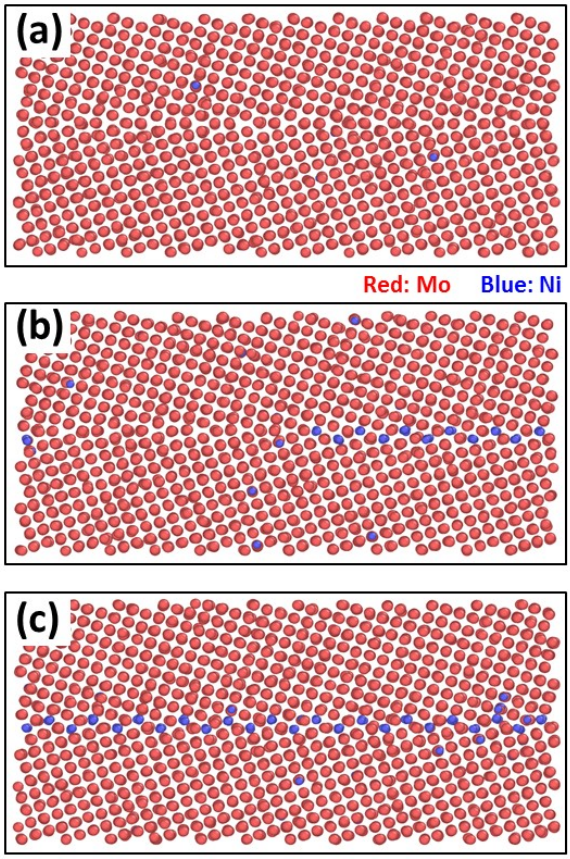

FIG. 1. Simulation of a GB phase-like transformation with increasing $\Delta\mu_{Ni}$ ($\equiv \mu_{Ni} - \mu_{Ni}^{(pure)}$) at a fixed temperature of $T = 0.373\ T_m$, showing **(a)** a nominally "clean" GB at a low $\Delta\mu_{Ni}$ of -0.56 eV/atom, **(b)** coexistence of two complexions at the transformation threshold $\Delta\mu_{Ni}$ of -0.435 eV/atom, and **(c)** a bilayer complexion (with disorder) at a high $\Delta\mu_{Ni}$ of -0.385 eV/atom. The corresponding GB structures at $T = 0$K without thermal noises (obtained by the modified GA) are shown in Supplemental Fig. S6.

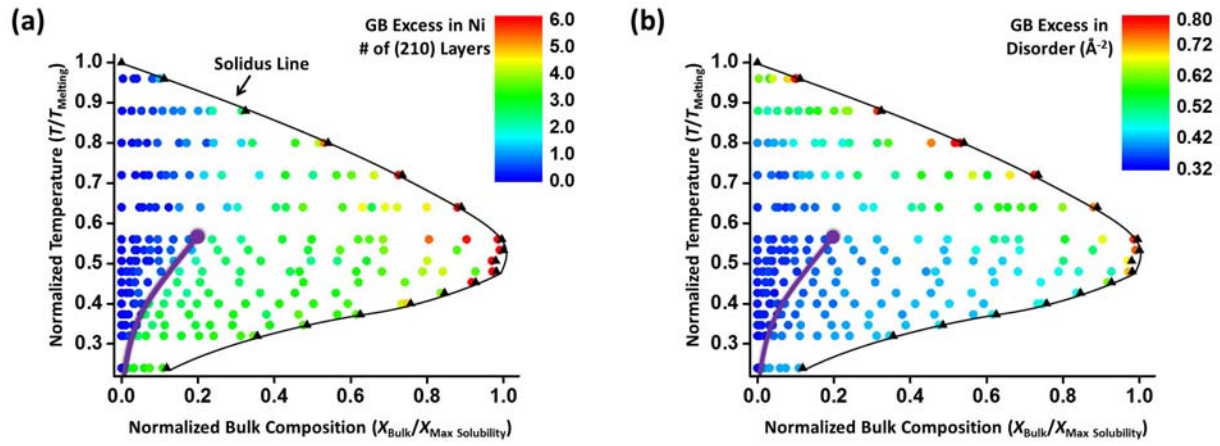

FIG. 2. Simulated GB complexion (phase) diagrams. **(a)** The computed map of GB adsorption from hybrid MC/MD simulations. **(b)** The computed map of GB excess disorder. The solid purple line represents first-order phase-like transformations and ends at a GB critical point.

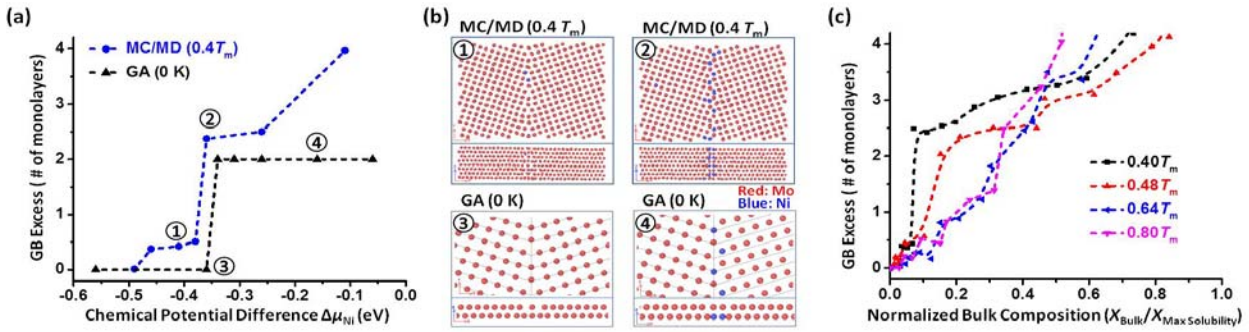

FIG. 3. The first-order phase-like transformations predicted from atomistic simulations. **(a)** GB excess in Ni (in number of equivalent (210) atomic layers) *vs*. the chemical potential difference ($\Delta\mu_{Ni} \equiv \mu_{Ni} - \mu_{Ni}^{(pure)}$) computed by both the hybrid MC/MD simulation at $T = 0.4T_m$ and the modified GA at $T = 0$ K. **(b)** The simulated GB atomic configurations (both top and side views) that correspond to the four points labeled in panel (a). **(c)** The variation of GB excess in Ni with the normalized bulk composition at four different temperatures computed from hybrid MC/MD simulations. The abrupt adsorption transition (from "$\Gamma_{Ni} = 0$" to "$\Gamma_{Ni} = 2$ monolayers" at 0K) shown in panel (a) occurs concurrently with a structural transition that breaks the mirror symmetry of the symmetric tilt GB, with a relative translation of the two abutting grains by a distance of $0.3 \cdot a_{bcc}$ along the vertical direction in panel (b) and asymmetric adsorption of the second Ni layer on (only) one abutting grain. In addition, the two abutting grains are closer (by $\sim 0.21 \cdot a_{bcc}$) after the structural transformation but there is no relative translation perpendicular to the projection plane. See Supplemental Fig. S6 for the detail of this structural transformation at T = 0K obtained by the GA. Similar transformations occur at finite temperatures with increasing effects of interfacial disordering and the transformation becomes continuous at high temperatures.

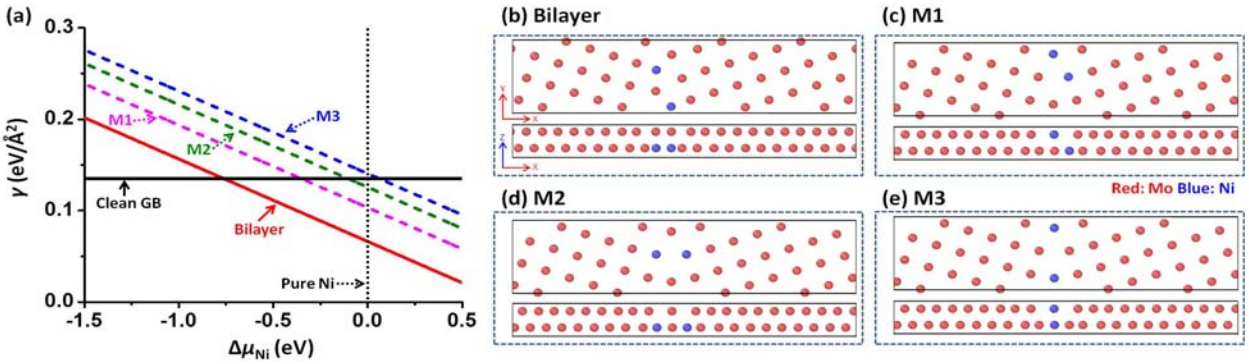

FIG. 4. DFT verification of the first-order transformation from the "clean" GB to the asymmetric bilayer complexion in Ni-doped Mo ∑5 (210) / [001] symmetric tilt GB. **(a)** GB energy computed by DFT *vs.* the chemical potential difference ($\Delta\mu_{Ni} \equiv \mu_{Ni} - \mu_{Ni}^{(pure)}$). Illustrations of **(b)** the bilayer GB structure produced by the modified GA and **(c, d, e)** several other possible GB structures (named as M1, M2, and M3, respectively). DFT calculations demonstrated that the asymmetric bilayer is the most stable adsorption structure among these four possible configuartions.